

An Efficient Gabor Feature-Based Multi-task Joint Support Vector Machines Framework for Hyperspectral Image Classification

Sen Jia^(✉) and Bin Deng^(✉)

College of Computer Science and Software Engineering,
Shenzhen University, Shenzhen, China
senjia@szu.edu.cn, szubing@qq.com

Abstract. In this paper, a novel multi-task learning (MTL) framework for a series of Gabor features via joint probabilistic outputs of support vector machines (SVM), abbreviated as GF-MTJSVM, has been proposed for Hyperspectral image (HSI) classification. Specifically, we firstly use a series of Gabor wavelet filters with different scales and frequencies to extract spectral-spatial-combined features from the HSI data. Then, we apply these Gabor features into the multi-task learning framework via joint probabilistic outputs of SVM. Experimental results on two widely used real HSI data indicate that the proposed GF-MTJSVM approach outperforms several well-known classification methods.

Keywords: Hyperspectral image classification · Multi-task support vector machines · Gabor features

1 Introduction

Hyperspectral sensors collect information as a set of images. Each image represents a narrow wavelength range of the electromagnetic spectrum, also known as a spectral band. Each pixel in a hyperspectral image (HSI) is a high-dimensional vector whose entries are the spectral responses of various spectral bands. The very informative spectral information of the HSI pixels can be utilized to distinguish objects in the image scene. As a major application of hyperspectral data analysis, pixel-oriented classification has been widely adopted [6, 22, 26]. In the hyperspectral supervised classification case, the class label of each pixel, denoted by a vector whose entries correspond to the narrow spectral band responses, is determined by a given training set from each class [5, 7, 13, 17]. To tackle the problem, many classifiers have been employed, including K-nearest neighbors (KNN)

This work was jointly supported by grants from National Natural Science Foundation of China (61671307 and 61271022), Guangdong Foundation of Outstanding Young Teachers in Higher Education Institutions (Yq2013143), Shenzhen Scientific Research and Development Funding Program (JCYJ20140418095735628, JCYJ20160422093647889 and SGLH20150206152559032).

[9], support vector machines (SVM) [8], sparse representation-based classification (SRC) [33]. However, due to the high dimensionality in spectral domain of HSI, finding optimal parameters for the supervised classifiers is time-consuming. Meanwhile, due to the extremely high spectral dimensionality of the data, the small sample size scenario (it is very difficult and time consuming to collect sufficient training samples in practice) is one crucial problem that limits the performance of many existing classification methods [18, 27].

Recently, many spectral-spatial classification methods in HSI have been proposed to improve the accuracy further. The spectral-spatial classification methods can be roughly divided into two categories. The first one is that the spectral and spatial contextual information is exploited separately, that is, the spatial dependencies are extracted through various spatial filters (such as morphological [3, 11, 14, 20], range [24], entropy [32], low-rank representation [36]) in advance, and then combined with the spectral features (or dimension reduced ones) to perform pixel-wise classification, or the spatial information is used to refine the classification results through a regularization process in the postprocessing stage [31], including Markov random field [30] and graph cuts [19]. However, a large number of training samples is generally required to adequately characterize the large variability of the objects, which is difficult to meet in most circumstances. The second one is that the spatial information is directly fused with the spectral features to produce joint features [21]. For example, a set of filters (such as wavelets [28], Gabor wavelets [2, 29]) can be applied on the hyperspectral data to extract spectral-spatial-combined features. Meanwhile, in recent years, multiple features combines to design a classifier has been a growing trend for the hyperspectral classification. It is obvious that multiple features can provide diverse information in characterizing object from different viewpoints. So it is always can achieve a better classification accuracy through combination of a set of modalities of features [35]. Several methods, such as Multiple Kernel Learning (MKL, in which the similarity functions between images are linearly combined) [15, 16], SVM ensemble (inspired by linearly programming Boosting) [12], have been developed for multi-class object classification. Zheng et al. [37] applied the multi-task joint sparse representation classification (MTJSRC) proposed in [35] with spatial filtering postprocessing into large-scale satellite image annotation and obtained excellent results. These methods all can obtained excellent results, but require either a large amount of computation time, or very complex model to construct a multi-task learning framework.

In this paper, a novel and simple multi-task learning (MTL) framework for a series of Gabor features via joint probabilistic outputs of SVM, called as GF-MTJSVM, was proposed for HSI classification. Firstly, a series of Gabor features were extracted by applying a set of predefined Gabor filters (with different scales and orientations) on the original hyperspectral data, which contains the wealth of information about signal changes in the local area, and provide an important classification identification information. Then, the multi-task learning via joint probabilistic outputs of SVM was applied for material identification. In the GF-MTJSVM framework, we simply combined category probabilistic outputs for the

SVM of each Gabor cube features as the final category probabilistic outputs. Experimental results on two real hyperspectral data with different spectral and spatial resolutions demonstrated the effectiveness of the proposed Gabor feature-based multi-task joint support vector machines Framework for hyperspectral image classification.

The rest of the paper is organized as follows. In Sect. 2, we introduce the basic Gabor filters and the classical support vector classification is described later on. Section 3 presents the proposed GF-MTJSVM approach, in detail. Experiment was run on two real hyperspectral data set and the results are shown in Sect. 4. Section 5 concludes the paper with a summary of the proposed work.

2 Related Work

2.1 Gabor Functions and Wavelets

Texture analysis has a long history and texture analysis algorithms range from using random field models to multiresolution filtering techniques such as the wavelet transform [23]. A two dimensional Gabor function $\Psi = (x, y)$ can be written as:

$$\Psi(x, y) = \left(\frac{1}{2\pi\sigma_x\sigma_y} \right) \exp \left[-\frac{1}{2} \left(\frac{x^2}{\sigma_x^2} + \frac{y^2}{\sigma_y^2} \right) + 2\pi j\omega x \right] \quad (1)$$

Gabor function form a complete but nonorthogonal basis set. Expanding a signal using this basis provides a localized frequency description. A class of self-similar functions, referred to as Gabor wavelets in the following discussion, is now considered. Let $\Psi(x, y)$ be the mother Gabor wavelet, then this self-similar filter dictionary can be obtained by appropriate dilations and rotations of $\Psi(x, y)$ through the generating function:

$$\begin{aligned} \Psi_{mn}(x, y) &= a^{-m} \Psi(x', y'), \quad a > 1, \quad m, n = \text{integer} \\ x' &= a^{-m} (x \cos \theta_n + y \sin \theta_n), \quad \text{and} \quad y' = a^{-m} (-x \sin \theta_n + y \cos \theta_n). \end{aligned} \quad (2)$$

Where $\theta_n = n\pi/K$ and K is the total number of orientations. The scale factor $S_m = a^{-m}$ in (2) is meant to ensure that the energy is independent of m . Through change the scaling size and the direction of rotation, we can get a group of Gabor wavelets.

2.2 Classical Support Vector Classification (C-SVC)

Given training vectors $\mathbf{x}_i \in \mathbb{R}^n, i = 1, \dots, l$, in two classes, and an indicator vector $\mathbf{y} \in \mathbb{R}^l$ such that $y_i \in \{1, -1\}$, C-SVC [4, 10] solves the following primal optimization problem:

$$\begin{aligned} \min_{\mathbf{w}, b, \xi} \quad & \frac{1}{2} \mathbf{w}^T \mathbf{w} + C \sum_{i=1}^l \xi_i \\ \text{subject to} \quad & y_i (\mathbf{w}^T \phi(\mathbf{x}_i) + b) \geq 1 - \xi_i, \\ & \xi_i \geq 0, i = 1, \dots, l. \end{aligned} \quad (3)$$

Where $\phi(\mathbf{x}_i)$ maps \mathbf{x}_i into a higher-dimensional space and $C > 0$ is the regularization parameter. Due to the possible high dimensionality of the vector variable \mathbf{w} , usually we solve the following dual problem:

$$\begin{aligned} \min_{\alpha} \quad & \frac{1}{2} \alpha^T \mathbf{Q} \alpha - \mathbf{e}^T \alpha \\ \text{subject to} \quad & \mathbf{y}^T \alpha = 0, \quad 0 \leq \alpha_i \leq C, i = 1, \dots, l. \end{aligned} \quad (4)$$

Where $\mathbf{e} = [1, \dots, 1]^T$ is the vector of all ones, \mathbf{Q} is an l by l positive semi-definite matrix, $\mathbf{Q}_{ij} \equiv y_i y_j \mathbf{K}(\mathbf{x}_i, \mathbf{x}_j) \equiv \phi(\mathbf{x}_i)^T \phi(\mathbf{x}_j)$ is the kernel function.

After problem 4 is solved, using the primal-dual relationship, the optimal \mathbf{w} satisfies:

$$\mathbf{w} = \sum_{i=1}^l y_i \alpha_i \phi(\mathbf{x}_i) \quad (5)$$

Then we can get the threshold output of a vector \mathbf{x} :

$$f(\mathbf{x}) = \sum_{i=1}^l y_i \alpha_i \mathbf{K}(\mathbf{x}_i, \mathbf{x}) + b. \quad (6)$$

And the decision function is:

$$h(\mathbf{x}) = \text{sgn}(f(\mathbf{x})). \quad (7)$$

3 Gabor Feature-Based Multi-task Joint Support Vector Machines for Hyperspectral Classification

After introducing the basic Gabor function and classical support vector classification in the previous section, a novel multi-task framework for hyperspectral classification, which is named the GF-MTJSVM, is proposed in this section. The framework GF-MTJSVM consists of two main steps, Gabor features extraction and combine the probabilistic outputs of SVM for each Gabor features. Figure 1 illustrates the schematic diagram of the proposed strategy.

3.1 Gabor Features Extraction for Hyperspectral Image

The nonorthogonality of Gabor wavelets implies that there is redundant information in the filtered images. In order to reduce this redundancy, B.S. Manjunathi et al. [23] proposed an effective strategy to design the Gabor filter dictionary. From the design of the Gabor filter dictionary, we can get a series of Gabor wavelet filters with different scales and frequencies. Denoted a set of 2-D Gabor filters as $\{\Psi_i, i = 1, 2, \dots, I\}$ (I is the number of Gabor filters) and the original hyperspectral data as $\mathbf{R} \in \mathbb{R}^{X \times Y \times B}$. For each Ψ_i at each spectral band λ , the magnitude $\mathbf{M}_i(x, y, \lambda) = |(\mathbf{R} * \Psi_i)(x, y)|$ contains rich signal change information around location (x, y) , where $*$ is the convolution operation, and $\mathbf{M}_i(x, y) = [\mathbf{M}_i(x, y, 1), \mathbf{M}_i(x, y, 2), \dots, \mathbf{M}_i(x, y, B)]$ is the responses of the i -th

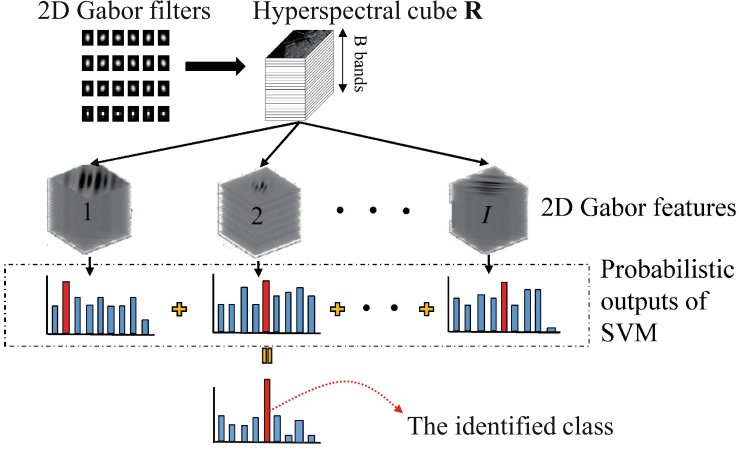


Fig. 1. Framework of GF-MTJSVM

Gabor filter at all bands. Through applying Ψ_i on all pixels of the hyperspectral image data, a Gabor cube $\mathbf{M}_i \in \mathbb{R}^{X \times Y \times B}$ can be obtained, which has the same size as the original hyperspectral data \mathbf{R} . Further, after each Gabor filter $\Psi_i, i = 1, 2, \dots, I$ has been convolved with the hyperspectral image data, a total of I Gabor cubes $\mathbf{M}_i, i = 1, 2, \dots, I$ were extracted.

3.2 Combine Probabilistic Outputs of SVM for Gabor Features

Given k classes of hyperspectral data $\mathbf{R} \in \mathbb{R}^{X \times Y \times B}$, and its corresponding i -th Gabor cube $\mathbf{M}_i \in \mathbb{R}^{X \times Y \times B}$ from Sect. 3.1. For each pixel $\mathbf{x} \in \mathbb{R}^B$ need to predict class label in the hyperspectral data \mathbf{R} , and the $\mathbf{x}^{(i)} \in \mathbb{R}^B$ is it corresponding i -th Gabor feature from Gabor cube \mathbf{M}_i , our first goal is to estimate

$$p_m^{(i)} = P(y = m | \mathbf{x}^{(i)}), \quad m = 1, \dots, k. \quad (8)$$

Following the setting of the one-against-one approach for multiclass classification, we first estimate pairwise class probabilities

$$r_{mn}^{(i)} \approx P(y = m | y = m \text{ or } n, \mathbf{x}^{(i)}) \quad (9)$$

If f_i is the decision value at $\mathbf{x}^{(i)}$ from the formula 6, then we assume

$$r_{mn}^{(i)} = \frac{1}{1 + e^{af_i + b}} \quad (10)$$

where a and b are estimated by minimizing the negative log likelihood of training data (using their labels and decision values) [25].

After collecting all $r_{mn}^{(i)}$ values, Wu et al. [34] propose two approaches to obtain $p_m^{(i)}, \forall m$. we consider their second approach and solve the following optimization problem.

$$\begin{aligned} \min_{\mathbf{p}^{(i)}} \quad & \frac{1}{2} \sum_{m=1}^k \sum_{n:n \neq m} \left(r_{nm}^{(i)} p_m^{(i)} - r_{mn}^{(i)} p_n^{(i)} \right)^2 \\ \text{subject to} \quad & p_m^{(i)} \geq 0, \forall m, \sum_{m=1}^k p_m^{(i)} = 1 \end{aligned} \quad (11)$$

Finally, the class label of \mathbf{x} is predicted to the class with the biggest total probability over all the I tasks, i.e.,

$$\text{Class}(\mathbf{x}) = \arg \max_m \sum_{i=1}^I p_m^{(i)} \quad (12)$$

Where I is the total number of the Gabor cubes.

4 Experimental Results

In this section, the performance of the proposed GF-MTJSVM method is tested in classification of two real hyperspectral imagery. The classification results are compared with state-of-the-art methods, i.e., support vector machines (SVM), sparse representation-based classification (SRC), and extended morphological and attribute profiles (EMAP) [11]. In the experiments, the Homotopy method is used to recover the sparse signals [1], the parameter of sparsity factor in SRC was set to be 0.01, while rbf-kernel and one-against-all scheme in SVM was used for the remaining methods. Besides, the C parameter of SVM is estimated by ten-fold cross validation. After the training set has been randomly partitioned into ten groups, nine groups are used to train a set of models that are evaluated on the remaining group. This procedure is then repeated for all ten possible choices for the held-out group, and the performance scores from the ten runs are then averaged. The performance of the compared techniques is evaluated with different samples (i.e., 5, 6, 7, ..., 15) are selected from each class to form the training set. And the remaining samples are then used as the test set for evaluation. Each experiment is repeated ten times with different training sets to reduce the influence of random effects, and both the mean and standard deviation are reported. In the experimental results, overall accuracy (OA) and kappa coefficient (κ) are used as measures of accuracy.

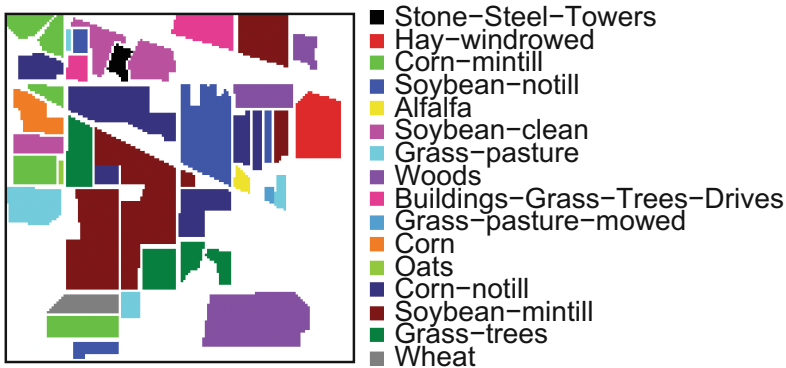
4.1 Indian Pines Data Set

The first real-world data set to be used is the commonly used Indian Pines data set acquired by the AVIRIS instrument over the agricultural area of Northwestern Indiana in 1992, which has a spatial dimension of 145×145 and 224 spectral

Table 1. Land cover classes with number of samples for the Indiana Pines data

Class	Land cover type	No. of samples
<i>C1</i>	Alfalfa	54
<i>C2</i>	Buildings-grass-trees-drives	380
<i>C3</i>	Corn	234
<i>C4</i>	Corn-min till	834
<i>C5</i>	Corn-no till	1434
<i>C6</i>	Grass-pasture-mowed	26
<i>C7</i>	Grass/pasture	497
<i>C8</i>	Grass/trees	747
<i>C9</i>	Hay-windrowed	489
<i>C10</i>	Oats	20
<i>C11</i>	Soybean-clean till	614
<i>C12</i>	Soybean-min till	2468
<i>C13</i>	Soybean-no till	968
<i>C14</i>	Soybean-steel-towers	95
<i>C15</i>	Wheat	212
<i>C16</i>	Woods	1294
	Total	10366

bands. The spatial resolution of the data is 20 m per pixel. After discarding 4 zero bands and the 35 lower SNR bands affected by atmospheric absorption, 185 channels are preserved. The data set contains 10366 labeled pixels and 16 ground-truth classes, most of which are different types of crops (see Table 1). Figure 2 shows the ground-truth map containing 16 mutually exclusive land-cover class.

**Fig. 2.** Ground-truth map of the Indian Pines data set (sixteen land cover classes).

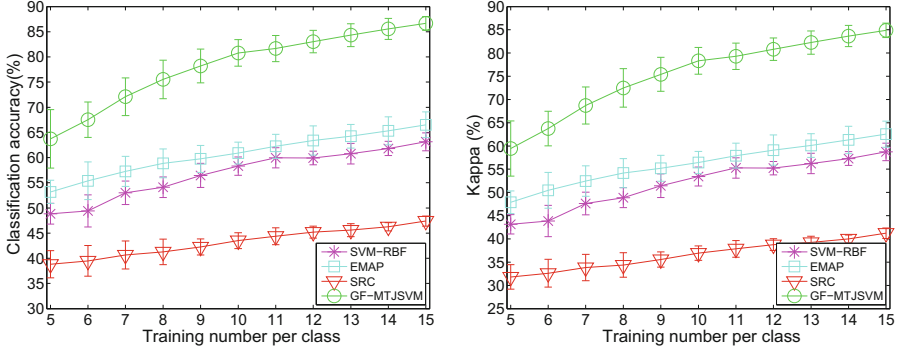


Fig. 3. Overall accuracy and kappa coefficient of the Indian Pines data set.

Figure 3 displays the overall accuracy (OA) and kappa coefficient measure as functions of the number of training samples per class (5, 6, 7, ..., 15). From the figure we can see, the performance of the GF-MTJSVM method is significantly higher than those methods (SVM, SRC, EMAP), demonstrating the superiority of the GF-MTJSVM framework.

Table 2. Land cover classes with number of samples for the Kennedy Space Center data

Class	Land cover type	No. of samples
C_1	Scrub	761
C_2	Willow swamp	243
C_3	Cabbage palm hammock	256
C_4	Cabbage palm/oak hammock	252
C_5	Slash pine	161
C_6	Oak/broadleaf hammock	229
C_7	Hardwood swamp	105
C_8	Graminoid marsh	431
C_9	Spartina marsh	520
C_{10}	Cattail marsh	404
C_{11}	Salt marsh	419
C_{12}	Mud flats	503
C_{13}	Water	927
	Total	5211

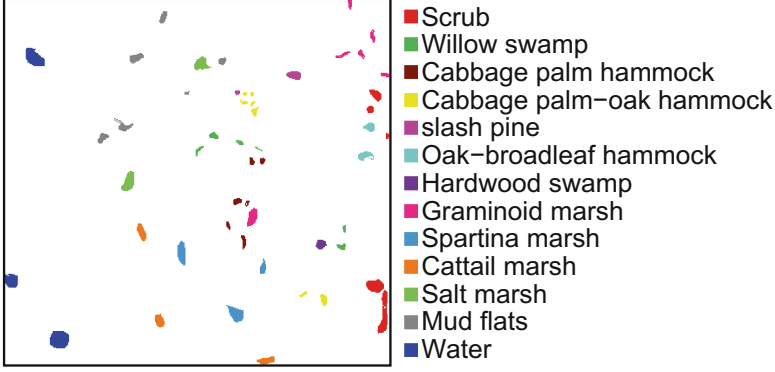


Fig. 4. Ground-truth map of the Kennedy Space Center data set (thirteen land cover classes).

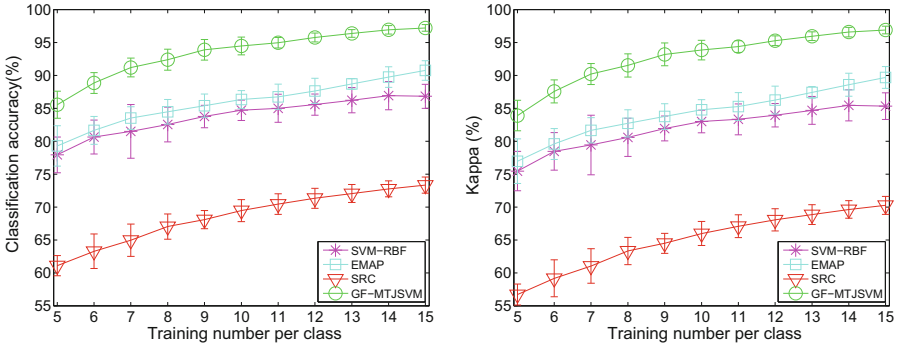


Fig. 5. Overall accuracy and kappa coefficient of the Kennedy Space Center data set.

4.2 KSC Data Set

The second data set that we used in our experiments was acquired by the AVIRIS sensor over the Kennedy Center (KSC), Merritt Island, FL, USA, on March 23, 1996. Figure 4 depicts the ground-truth map of the land covers. In the original 224 bands, 48 bands are identified as water absorption and low-SNR bands (numbered 1–4, 102–116, 151–172, and 218–224), which are discarded, and only 176 bands remain. The spatial resolution of the data is 18m per pixel. For classification purposes, 13 classes representing the various land-cover types that occur in this environment were defined for the site (see Table 2).

Figure 5 displays the overall accuracy (OA) and kappa coefficient measure as functions of the number of training samples per class (5, 6, 7, ..., 15). Same as the first experiment, the results obtained by our GF-MTJSVM method are more accurate than those of the other three ones. For these two experimental both demonstrating the superiority of the GF-MTJSVM framework.

5 Conclusion

In this paper, we propose the GF-MTJSVM framework for hyperspectral image classification. We observe that the multi-task joint support vector machines is a simple yet effective way to fuse multiple complementary Gabor features to improve the classification accuracy for the small training sample classification task. Experiments on two real-world hyperspectral data show that our method performs quite competitive to several representative state-of-the-art methods. In summary, we can conclude with observations that Gabor feature-based multi-task joint support vector machines is an effective method for hyperspectral image classification with small training sample.

References

1. Asif, M.S.: Dynamic compressive sensing: sparse recovery algorithms for streaming signals and video. Ph.D. thesis, Georgia Institute of Technology (2013)
2. Bau, T.C., Sarkar, S., Healey, G.: Hyperspectral region classification using a three-dimensional Gabor filterbank. *IEEE Trans. Geosci. Remote Sens.* **48**(9), 3457–3464 (2010)
3. Benediktsson, J.A., Palmason, J.A., Sveinsson, J.R.: Classification of hyperspectral data from urban areas based on extended morphological profiles. *IEEE Trans. Geosci. Remote Sens.* **43**(3), 480–491 (2005)
4. Boser, B.E., Guyon, I.M., Vapnik, V.N.: A training algorithm for optimal margin classifiers. In: *Proceedings of the Fifth Annual Workshop on Computational Learning Theory*, pp. 144–152. ACM (1992)
5. Camps-Valls, G., Bruzzone, L.: Kernel-based methods for hyperspectral image classification. *IEEE Trans. Geosci. Remote Sens.* **43**(6), 1351–1362 (2005)
6. Chang, C.I.: *Hyperspectral Imaging: Techniques for Spectral Detection and Classification*, vol. 1. Springer, New York (2003)
7. Chang, C.I.: *Hyperspectral Data Exploitation: Theory and Applications*. Wiley, Chichester (2007)
8. Chang, C.C., Lin, C.J.: LIBSVM: a library for support vector machines. *ACM Trans. Intell. Syst. Technol. (TIST)* **2**(3), 27 (2011)
9. Chen, Y., Lin, Z., Zhao, X.: Riemannian manifold learning based k-nearest-neighbor for hyperspectral image classification. In: *IEEE International Geoscience and Remote Sensing Symposium (IGARSS)*, pp. 1975–1978 (2013)
10. Cortes, C., Vapnik, V.: Support-vector networks. *Machine Learn.* **20**(3), 273–297 (1995)
11. Dalla Mura, M., Atli Benediktsson, J., Waske, B., Bruzzone, L.: Extended profiles with morphological attribute filters for the analysis of hyperspectral data. *Int. J. Remote Sens.* **31**(22), 5975–5991 (2010)
12. Gehler, P., Nowozin, S.: On feature combination for multiclass object classification. In: *2009 IEEE 12th International Conference on Computer Vision*, pp. 221–228. IEEE (2009)
13. Genc, L., Inalpulat, M., Kizil, U., Mirik, M., Smith, S.E., Mendes, M.: Determination of water stress with spectral reflectance on sweet corn (*Zea mays* L.) using classification tree (CT) analysis. *Zemdirbyste Agric.* **100**(1), 81–90 (2013)

14. Ghamisi, P., Dalla-Mura, M., Benediktsson, J.: A survey on spectral-spatial classification techniques based on attribute profiles. *IEEE Trans. Geosci. Remote Sens.* **53**(5), 2335–2353 (2015)
15. Gu, Y., Gao, G., Zuo, D., You, D.: Model selection and classification with multiple kernel learning for hyperspectral images via sparsity. *IEEE J. Sel. Top. Appl. Earth Observ. Remote Sensing*, **7**(6), 2119–2130 (2014)
16. Gu, Y., Wang, C., You, D., Zhang, Y., Wang, S., Zhang, Y.: Representative multiple kernel learning for classification in hyperspectral imagery. *IEEE Trans. Geosci. Remote Sens.* **50**(7), 2852–2865 (2012)
17. Harsanyi, J.C., Chang, C.I.: Hyperspectral image classification and dimensionality reduction: an orthogonal subspace projection approach. *IEEE Trans. Geosci. Remote Sens.* **32**(4), 779–785 (1994)
18. Lee, M.A., Prasad, S., Bruce, L.M., West, T.R., Reynolds, D., Irby, T., Kalluri, H.: Sensitivity of hyperspectral classification algorithms to training sample size. In: *First Workshop on Hyperspectral Image and Signal Processing: Evolution in Remote Sensing, WHISPERS 2009*, pp. 1–4. IEEE (2009)
19. Li, J., Bioucas-Dias, J.M., Plaza, A.: Semisupervised hyperspectral image segmentation using multinomial logistic regression with active learning. *IEEE Trans. Geosci. Remote Sens.* **48**(11), 4085–4098 (2010)
20. Li, J., Huang, X., Gamba, P., Bioucas-Dias, J., Zhang, L., Atli-Benediktsson, J., Plaza, A.: Multiple feature learning for hyperspectral image classification. *IEEE Trans. Geosci. Remote Sens.* **53**(3), 1592–1606 (2015)
21. Li, J., Marpu, P.R., Plaza, A., Bioucas-Dias, J.M., Benediktsson, J.A.: Generalized composite kernel framework for hyperspectral image classification. *IEEE Trans. Geosci. Remote Sens.* **51**(9), 4816–4829 (2013)
22. Lu, D., Weng, Q.: A survey of image classification methods and techniques for improving classification performance. *Int. J. Remote Sens.* **28**(5), 823–870 (2007)
23. Manjunath, B.S., Ma, W.Y.: Texture features for browsing and retrieval of image data. *IEEE Trans. Pattern Anal. Mach. Intell.* **18**(8), 837–842 (1996)
24. Pacifici, F., Chini, M., Emery, W.J.: A neural network approach using multi-scale textural metrics from very high-resolution panchromatic imagery for urban land-use classification. *Remote Sens. Environ.* **113**(6), 1276–1292 (2009)
25. Platt, J., et al.: Probabilistic outputs for support vector machines and comparisons to regularized likelihood methods. *Advances Large Margin Classif.* **10**(3), 61–74 (1999)
26. Plaza, A., Benediktsson, J.A., Boardman, J.W., Brazile, J., Bruzzone, L., Camps-Valls, G., Chanussot, J., Fauvel, M., Gamba, P., Gualtieri, A., et al.: Recent advances in techniques for hyperspectral image processing. *Remote Sens. Environ.* **113**, S110–S122 (2009)
27. Prasad, S., Bruce, L.M.: Overcoming the small sample size problem in hyperspectral classification and detection tasks. In: *IEEE International Geoscience and Remote Sensing Symposium, IGARSS 2008*. vol. 5, pp. V-381. IEEE (2008)
28. Qian, Y., Ye, M., Zhou, J.: Hyperspectral image classification based on structured sparse logistic regression and three-dimensional wavelet texture features. *IEEE Trans. Geosci. Remote Sens.* **51**(4), 2276–2291 (2013)
29. Shen, L., Jia, S.: Three-dimensional gabor wavelets for pixel-based hyperspectral imagery classification. *IEEE Trans. Geosci. Remote Sens.* **49**(12), 5039–5046 (2011)
30. Tarabalka, Y., Fauvel, M., Chanussot, J., Benediktsson, J.A.: SVM- and MRF-based method for accurate classification of hyperspectral images. *IEEE Trans. Geosci. Remote Sens.* **7**(4), 736–740 (2010)

31. Tarabalka, Y., Chanussot, J., Benediktsson, J.A.: Segmentation and classification of hyperspectral images using watershed transformation. *Pattern Recogn.* **43**(7), 2367–2379 (2010)
32. Tuia, D., Volpi, M., Dalla Mura, M., Rakotomamonjy, A., Flamary, R.: Automatic feature learning for spatio-spectral image classification with sparse. *SVM* **52**(10), 6062–6074 (2014)
33. Wright, J., Yang, A.Y., Ganesh, A., Sastry, S.S., Ma, Y.: Robust face recognition via sparse representation. *IEEE Trans. Pattern Anal. Mach. Intell.* **31**(2), 210–227 (2009)
34. Wu, T.F., Lin, C.J., Weng, R.C.: Probability estimates for multi-class classification by pairwise coupling. *J. Mach. Learn. Res.* **5**, 975–1005 (2004)
35. Yuan, X.T., Liu, X., Yan, S.: Visual classification with multitask joint sparse representation. *IEEE Trans. Image Process.* **21**(10), 4349–4360 (2012)
36. Zhao, Y.Q., Yang, J.: Hyperspectral image denoising via sparse representation and low-rank constraint. *IEEE Trans. Geosci. Remote Sens.* **53**(1), 296–308 (2015)
37. Zheng, X., Sun, X., Fu, K., Wang, H.: Automatic annotation of satellite images via multifeature joint sparse coding with spatial relation constraint. *IEEE Geosci. Remote Sens. Lett.* **10**(4), 652–656 (2013)

Pattern Recognition

7th Chinese Conference, CCPR 2016, Chengdu, China,

November 5-7, 2016, Proceedings, Part II

Tan, T.; Li, X.; Chen, X.; Zhou, J.; Yang, J.; Cheng, H.

(Eds.)

2016, XXIII, 735 p. 311 illus., Softcover

ISBN: 978-981-10-3004-8